CARBON 73 (2014) 25–33

Available at www.sciencedirect.com

ScienceDirect

journal homepage: www.elsevier.com/locate/carbon

Plasma-induced photoresponse in few-layer graphene

Kaliannan Thiyagarajan [a], Antony Ananth [b], Balasubramaniam Saravanakumar [a], Young Sun Mok [b], Sang-Jae Kim [a,*]

[a] Nanomaterials and System Lab, Department of Mechatronics Engineering, Jeju National University, Jeju 690 756, Republic of Korea
[b] Plasma Applications Laboratory, Department of Chemical and Biological Engineering, Jeju National University, Jeju 690 756, Republic of Korea

ARTICLE INFO

Article history:
Received 8 October 2013
Accepted 8 February 2014
Available online 13 February 2014

ABSTRACT

A device consisting of a few layers of graphene (FLG) sheets was exposed to atmospheric plasma, resulting in the generation of significant number of defects, oxygen absorption, and doping. The plasma-induced electrical transformation and photoconducting properties of pristine FLG and plasma-irradiated FLG (p-FLG) were compared under visible and ultraviolet (UV) light illumination. The visible light photoresponsivity of p-FLG was 0.47 AW^{-1} at 535 nm, comparatively higher than that observed for pristine FLG (10 m AW^{-1}); this result was attributed to the formation of defect midgap states band by plasma irradiation. Photoinduced molecular desorption causes the responsivity of the higher energy (UV) photons. Our results suggest that plasma irradiation is a simple, novel way to tailor the optoelectronic properties of graphene layers.

1. Introduction

Graphene is a fascinating one atom thick, two-dimensional (2-D) material, consisting of sp^2 hybridized carbon atoms arranged in a honeycomb structure. This material has been studied extensively due to its high electron mobility, optical transparency, flexibility, mechanical strength, and environmental stability [1–3]. The photoinduced responses of graphene and its associated composite materials in the form of photodetectors and phototransistors have been widely studied in recent years. Although single-layer graphene is an exceptional material with controlled electronic properties, it weakly absorbs absorbs light (e.g., single-layer graphene absorbs only 2.3% of incident light), which is a major drawback for the development of graphene-based photodetectors [4]. A number of experimental methods have been proposed to enhance the photoresponsivity of monolayer graphene, including increasing the absorption efficiency and lifetime (few picoseconds) of photo-generated carriers by exploiting the thermoelectric effect [4–6], metallic plasmonics [7], graphene plasmons [8,9], micro-cavities [10–12], and graphene quantum dots [13]. In contrast, photodetectors with quantum dots strongly, adsorbs light; however the photoconductive gain is limited (1×10^2–1×10^3) [14], due to the low mobility of charge carriers in quantum dots. To overcome these problems, Konstantatos et al. developed a hybrid phototransistor that combined the excellent electronic properties of graphene (high mobility of up to 60,000 $cm^2 V^{-1} s^{-1}$ at room temperature) with the optical properties of colloidal quantum dots (PbS), which yield a higher photoconductive gain of $\sim 10^8$ electrons per photon [15]. The sensitivity of the photodetector depended on the charge carriers present at the surface to

* *Corresponding author:* Fax: +82 64 756 3886.
E-mail address: kimsangj@jejunu.ac.kr (S.-J. Kim).
http://dx.doi.org/10.1016/j.carbon.2014.02.027
0008-6223/

respond to the incident photons (IP). Broad spectral bandwidth and fast response times make graphene an ideal material for optoelectronic and photodetector applications [15,16].

Tailoring the property of solid materials with ion irradiation and collision cascades is a method that has been used for several decades [17]. Defect engineering is one way to create a bandgap in graphene to manipulate its electrical, chemical, and magnetic properties. To engineer the electronic properties of graphene, researchers introduced artificial defects to the graphene surface by ion-beam irradiation (Ga^+ and Ar^+) [18,19]. Another approach is plasma irradiation, a novel method used to introduce defects and to dope the hydrophobic (chemically inert) graphene surface [20,21].

Here, we introduce a novel method to induce photoresponse from just a few layers of graphene (FLG) through artificial defects generation resulting from atmospheric plasma irradiation. The defect-induced electrical changes and photoconductive properties of pristine FLG and plasma-irradiated FLG (p-FLG) were studied under both visible (535 and 405 nm), UV (365 nm) light illumination by introducing a defect midgap states band (MGB). The higher photoresponsivity of $\sim$0.47 AW^{-1} for p-FLG was achieved using visible 535 nm light. This suggests plasma irradiation as an efficient tool for tailoring the optical and electrical properties of graphene.

2. Experimental section

Few-layer graphene sheets were peeled from highly oriented pyrolytic graphite (HOPG) using the scotch-tape method and transferred to a SiO_2/Si substrate. A gold (Au) electrode 100 nm in thickness was formed using a conventional photolithographic process, followed by thermal evaporation and the lift-off process (details of the lithographic process and thickness approximation procedure are given in Supplementary information). The fabricated FLG devices were annealed at 250 °C in Ar/H_2 atmosphere for 30 min to improve the adhesion of the gold electrodes with the graphene flake and to remove the residual resist. Prior to plasma exposure, electrodes were covered with epoxy resin and dried at 150 °C for 30 min in air to prevent electrode oxidization and damage. The FLG device was exposed to a homemade atmospheric plasma reactor (shown in Fig. S1a) for 5 min in an Ar atmosphere (flow rate of 60 sccm) at a pressure of $\sim$1 Torr. Fig. S1b shows a photograph of the Ar plasma generated. The effect of plasma irradiation on the FLG surface was clearly observed in the optical microscope images shown in Fig. S1c and d (before and after plasma irradiation, respectively). Raman spectroscopy measurements were performed using a 514 nm Ar^+ ion laser as an excitation light source (Horiba Jobin Yvon LabRAM HR800 system). Nanoview surface profile analysis (Nano System Co., Ltd) was employed to visualize the surface defects. The morphology was characterized using atomic force microscopy (AFM) with XE-100, park system. Foreign body attachment on p-FLG was confirmed by X-ray photoelectron spectroscopy (XPS) using an ESCA-2000, VG Microtech Ltd. spectrometer (Al Kα). Electrical and photocurrent measurements were carried out using a semiconductor parameter analyzer (Agilent, B 1500A) combined with a Prizmatix multi-wavelength LED light source.

3. Results and discussion

Defects are good when they enhance the material's properties in useful ways. Plasma and ion irradiation on the hydrophobic graphene (solid material) can induce different types of surface defects (e.g., vacancies, graphene islands, doping and impurity) [22,23]. Plasma irradiation disrupts honeycombed lattice to form vacancies [24], resulting in a highly disordered morphology (see Fig. S1d); the degree of disorder appears to be dependent on the thickness of the graphene flake [25]. The defect generation deteriorates the electrical conductivity of the graphene layers, even though its opens up several exciting applications in two-dimensional nanoelectronics.

To evaluate the tantalizing defect behavior of the p-FLG device, we studied its Raman spectrum. Fig. 1b shows the normalized Raman spectrum of a p-FLG device, along with a pristine FLG device. An optical microscopy image of a typical device is shown in the inset of Fig. 1b (circles indicate the measurement sites). The defect peaks (D, D′) associated with disorder were hardly noticeable in pristine FLG, however, strong peaks were observed at $\sim$1364 cm^{-1} (D peak) and 1624 cm^{-1} (D′ peak) after plasma exposure. The existence of intervalley (D) and intravalley (D′) phonons strongly indicates defect formation on the graphene surface. Similar results were observed previously for ozone exposure [3], oxygen plasma exposure [26], Ga^+ ion irradiation [20] and electron-beam irradiation [27] on single-layer graphene. To study the detailed defect generation at the graphene surface, we measured the Raman spectrum at different places on the graphene surface (e.g., the hub and the edge). The Raman spectrum of these distinct sites showed similar behavior, although with different intensities. The results clearly indicated that the defects levels were present more at the edges than the hub, which was in good agreement with the I_D/I_G ratios given in Table S1 (Supplementary information). This may be attributed to fewer graphene layers and different morphologies at the edges. The wavy degradation nature of graphene opens up novel applications in graphene research. These defects may act as light-absorbing site for optoelectronic applications.

To visualize the pristine FLG surface and wavy degradation nature of p-FLG, we used a non-destructive, non-contact, three-dimensional (3-D) nanoprofile measurement, (Fig. 2). Pristine FLG showed a smooth, defect-free surface with a roughness of 0.46 nm (Fig. 2a–c). These measurements were in good agreement with Raman spectroscopy. Apparently, plasma irradiation induced defects on the FLG surface, e.g., graphene islands and graphene dots, which increased the surface roughness value to 78 nm (Fig. 2d–f); the line profile in Fig. 2e, shows defect formation clearly. The results shown in Fig. 2f indicate that the graphene layers are not removed completely, only the plasma irradiation induces the defects on the p-FLG surface.

The morphology of the p-FLG was characterized using atomic force microscopy (AFM); and result is presented in Fig. 3. The morphology of the p-FLG is distinct from the pristine-FLG [18] which exhibits a relatively flat surface (see Supplementary information SI 2 and Fig. S2), when compare to the p-FLG. Graphene exposed to plasma generally causing two important differences on surface (i) generating surface

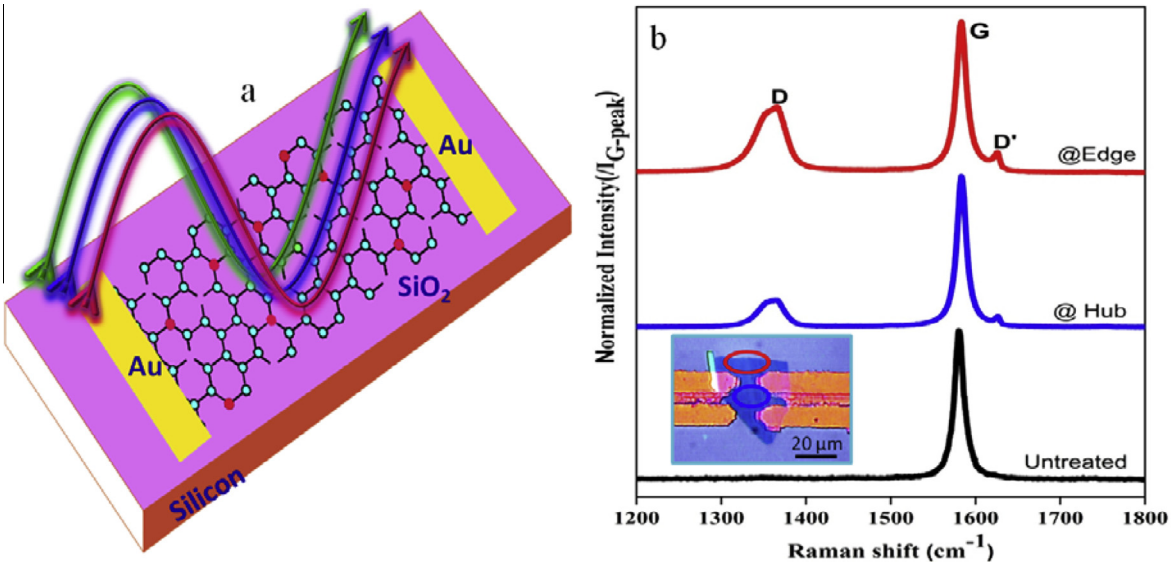

Fig. 1 – (a) Schematic representation of the plasma-irradiated graphene device. (b) The normalized micro Raman spectrum (λ = 532 nm) of the pristine few-layer graphene (FLG) sheets and plasma-irradiated (p-FLG) devices. The inset is an optical microscopy image of a typical device, where the circles indicate the measurement sites: hub (blue circle) and edge (red circle). (A colour version of this figure can be viewed online.)

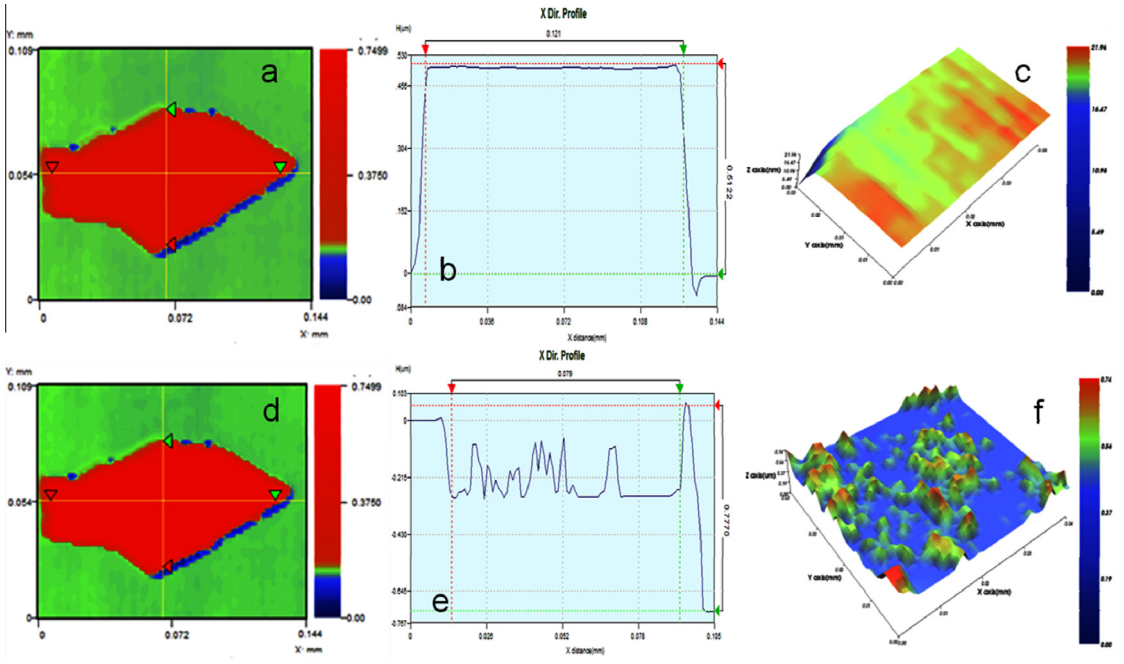

Fig. 2 – Surface profile analysis: (a) two-dimensional (2-D) image of FLG before plasma irradiation. (b) Line profile image corresponding to the *x*-axis of (a). (c) Three-dimensional (3-D) image showing the defect-free (uniform) surface. (d) 2-D image of plasma-irradiated FLG (i.e., the formation of p-FLG). (e) Line profile image corresponding to the *x*-axis of (d). (f) 3-D image showing defect formation on p-FLG. (A colour version of this figure can be viewed online.)

roughness, and (ii) blister formation (only for the prolonged plasma irradiation) [28]. Fig. 3c is the 2D image of the p-FLG and the corresponding line profile image is given in Fig. 3e, in which the height variation clearly indicates that the plasma irradiation induces defect on the graphene surface. The 3D image of p-FLG (Fig. 3d) is processed using image processing software (SPIP 6.2.5) and shown in Fig. 3f, which certainly serves as a evident for the formation of nano size defect hole (nano hole) on p-FLG surface and the depth of these defect holes is around 0.1–0.5 nm. These defects were contribute to the defect related D and D′ peaks of the Raman spectrum. Optical microscopy images, surface profile analysis, AFM analysis, and Raman spectroscopy conform that the plasma irradiation induces defect on graphene surface.

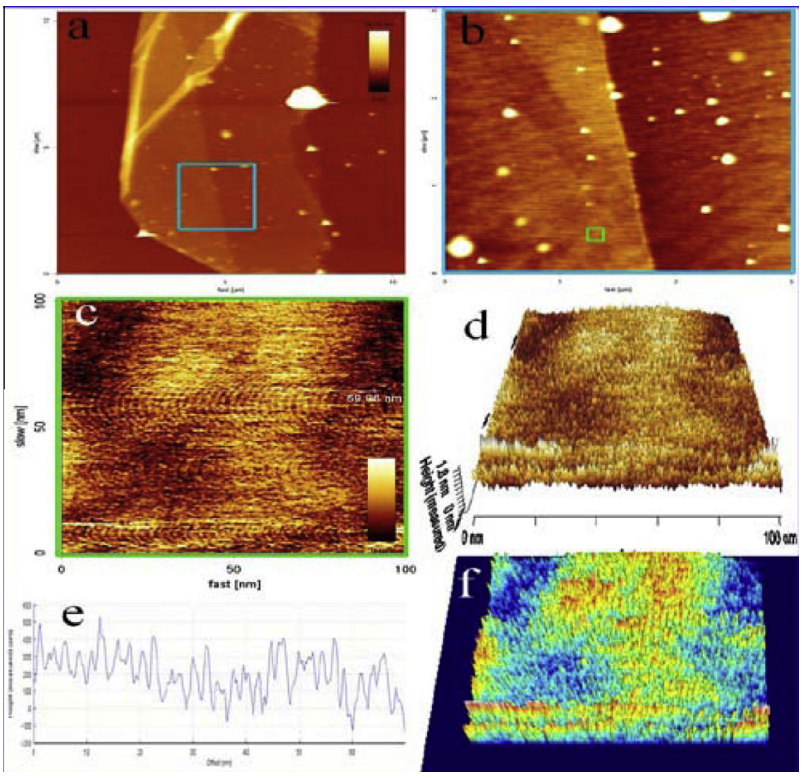

Fig. 3 – AFM analysis: (a, b) two-dimensional (2-D) image of p-FLG with different magnification. (c) 2-D image of the p-FLG at small scan area of (100 nm) and the corresponding three-dimensional (3-D) image shown in (d). (e) Line profile image corresponding to the x-axis of (c). (f) Processed 3-D image of (d) showing the nano hole defect formation on p-FLG. (A colour version of this figure can be viewed online.)

To confirm the attachment of a foreign body (oxygen bonding) to the surface of a p-FLG device, XPS measurement, was carried out. Different components of the XPS spectrum were deconvoluted using the Shirley method of background removal in conjunction with a least squares fitting algorithm using full Voigt functions. Fig. 4a and b correspond to the C 1s core level of the XPS spectra of FLG before and after plasma irradiation, respectively. The XPS results for pristine FLG revealed two different carbon bonds, as indicated by the peaks in Fig. 4a. The peak at 284.6 eV was attributed to sp^2 carbon (C=C/C—C) bonds [29–31], and the other peak at 285.8 eV was assigned to C—O bond that may arise during device

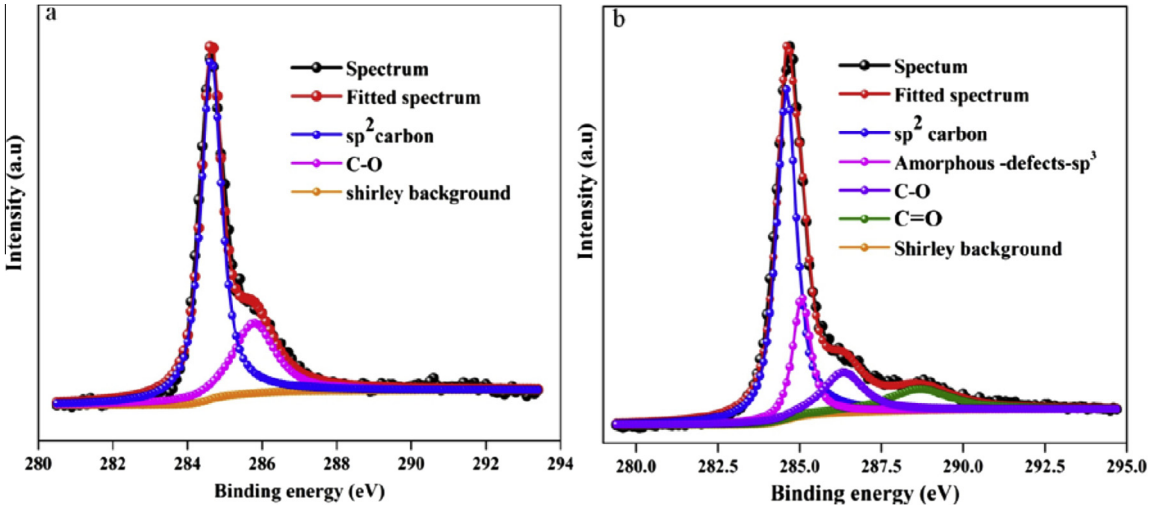

Fig. 4 – C1s high-resolution XPS spectra of the FLG device (a) before and (b) after plasma irradiation. Components related to various chemical shifts of the carbon bonds are indicated. (Note that the spectra were deconvoluted using the Shirley method of background removal). (A colour version of this figure can be viewed online.)

fabrication [32]. Fig. 4b is the XPS spectra of p-FLG. The peak at 284.6 eV corresponds to the sp^2 carbon (C=C/C—C) bonds [29,30], and the peak at 285.0 eV is ascribed to the sp^3 carbon due to amorphous defect generation (removal of carbon atoms from the honeycombed lattice) [19,33,34]; an increment in the peak intensity suggested that the surface was affected by plasma irradiation. The additional two peaks at 286.3 and 288.5 eV were attributed to C—O (epoxy/hydroxyl bonds) [28,35] and C=O (carbonyl bonds) [22,32,36] soon after defect generation, oxygen molecules from the atmosphere reacts with defected graphene surface to produce O-containing groups [21]. These results imply that chemical bonds have been formed between carbon and oxygen when FLG was exposed to atmospheric plasma.

The photoresponsivity of the pure graphene photodetector was low; we attributed this result to the poor absorption efficiency and short recombination lifetimes (few picoseconds) of the photo-generated carriers [37]. To date, few studies have investigated photocurrent generation in graphene based on carrier multiexcitation generation (MEG) (i.e., multiple charge carriers generated from the absorption of a single photon by impact ionization), also known as inverse Auger recombination (AR) [13,38,39]. Plasma irradiation on FLG tends to induce surface defect or vacancy formation, such as graphene quantum dots, graphene islands, and doping as well as deposit the impurities on hydrophobic graphene [23]. The underlying graphene layers serve as a transport layer, where the edges (having more defects) eventually follows percolative conduction path mechanism [3]. The defects, dopant (oxygen), and impurities are acting as light-absorbing centers, whereas graphene quantum dots or islands frame the MGB which behaves as an electron-trapping center, and a bandgap is created due to the quantum confinement.

Fig. 5a shows the energy band diagram for photocurrent generation in p-FLG. The IP generates an electron–hole pair through photo-excitation (PE) after impact ionization (II) (red arrows). The photo-excited electron relaxes to a lower-energy state inside the conduction band via an intraband transition simultaneously; an interband transition occurs that stimulates excitation of a valence band electron to the conduction band. Concurrently, electrons in the conduction band are scattered to the valence band by transferring energy to another electron present in the conduction band, which is ultimately excited to a higher-energy level by the AR process (black arrows Fig. 5a). Thus carrier multiplication was accomplished through impact ionization (II) and AR process [40,41], which produces secondary electrons in the conduction band. Once the band gap formed between the conduction and

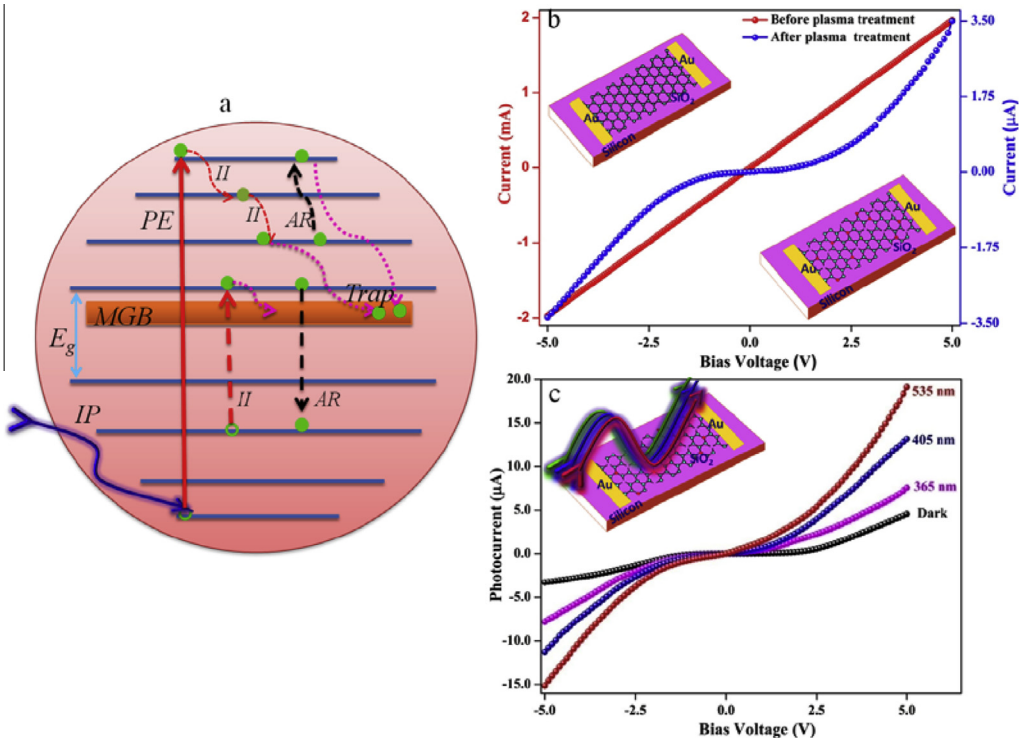

Fig. 5 – (a) Energy band diagram (including the defect midgap states band (MGB) and band gap energy (Eg)), including the concept for photocurrent generation for p-FLG. An incident photons (IP) interacts with the electron in the valence band and generates an electron–hole pair via photon excitation (PE), followed by the impact ionization (II) process. When the excited electron transfers to the lower energy level in the conduction band and transfers the energy to another electron, initiating the AR process. Each of the steps in this cascade increases the population of electron–hole pairs; the multiexcitation generation (MEG) effect exists, possibility of more excited electrons being trapped by the MGB. (b) Current (*I*) versus voltage (*V*) curve for FLG, before (red) and after (blue) plasma irradiation; the insets are the corresponding device structures before (top-left) and after (lower-right) plasma irradiation. (c) The photoresponse *I*–*V* curve of the p-FLG device under dark conditions and also with various light sources. The inset shows a schematic diagram of the p-FLG device interacting with light source. (A colour version of this figure can be viewed online.)

valence bands; the electron–phonon scattering decreases [42], which results in more photo-excited and secondary generated electrons trapping in MGB. The photo-generated hole is recirculated through hopping within the lifetime, which results in a high photoconductive gain.

Fig. 5b shows the current–voltage (*I–V*) characteristics of FLG before (red) and after (blue) plasma irradiation; the insets are the corresponding device structures before (top-left) and after (lower right) plasma irradiation. The pristine FLG device exhibited linear (Ohmic) *I–V* behavior with high electrical conductivity. After plasma irradiation (i.e., the formation of p-FLG), the device conductivity deteriorated considerably, exhibiting nonlinear behavior (Schottky). This behavior was attributed to the detachment of carbon atoms from the honeycomb lattice, the doping of oxygen, breaking of the π—π bond, and void formation, leading to the production of a vast number of graphene quantum dots, which absorb the incident light more efficiently than does pristine graphene. The layers with most defects ultimately results in a percolative conduction path for the applied bias voltage. To explore the plasma-induced photoresponse characteristics of the FLG device, we carried out photoelectric measurements under ambient conditions and an applied bias of −5 to 5 V for different illumination wavelengths (Fig. 5c). As a reference, we also measured the pristine FLG device under the same conditions. No obvious response was observed, which was expected due to the higher transmittance of defect-free graphene; however, the p-FLG device showed a strong dependence on illumination wavelength (see Fig. 5b and c). The maximum photocurrent was observed under 535 nm illumination; the photocurrent decreased with the illumination wavelength. The device illuminated with 365 nm photocurrent ($I_{\text{light-365 nm}}$) exhibited a maximum photocurrent of 7.67 μA, and the photocurrent $I_{\text{light-405 nm}}$ and $I_{\text{light-535 nm}}$ improved to 13.31 and 19.16 μA for the 405 and 535 nm wavelengths, respectively, under an applied bias voltage of 5 V.

Fig. 6a shows the time-dependent photocurrent measurement of the p-FLG device under UV (365 nm) and visible (405 and 535 nm) light irradiation at 0 V bias, with multiple on/off cycles. The turn-on and turn-off time of the light source was 10 s. The device exhibited excellent stability and reproducibility over the UV and visible region. When the light source was turned on, the photocurrent reached its maximum within a millisecond (ms). The ratio I_{light} to I_{dark} increased as the illumination wavelength, increased, having values of 90, 100, and 227, for wavelengths 365, 405, and 535 nm, respectively. The incident power dependence; and photocurrent for p-FLG are shown in Fig. 6b–d at different wavelength illuminations. Linear behavior was observed for the visible and UV wavelengths, indicating the broader spectral response of graphene.

The summarized photoresponse result of the p-FLG device is presented in Fig. 7. The response and recovery time of the device with respect to illumination wavelength is shown in Fig. 6a; the response and recovery time increased linearly with the illumination wavelength. The high-energy (365 nm) photons reduce the depletion barrier in a shorter time than

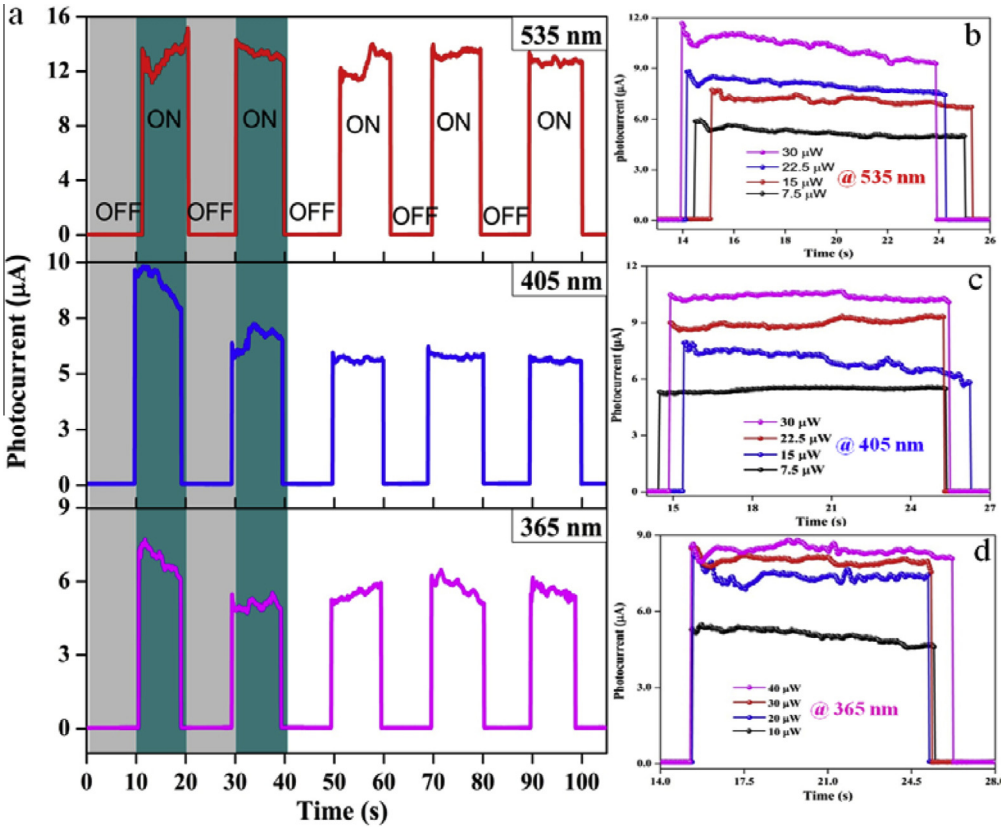

Fig. 6 – (a) Time-dependent photocurrent spectra of the p-FLG device under UV (365 nm) and visible (405 and 535 nm) light irradiation for a bias of 0 V, with multiple on/off cycles. The power dependence photocurrents for (b) 535, (c) 405, and (d) 365 nm at 0 V bias voltage. (A colour version of this figure can be viewed online.)

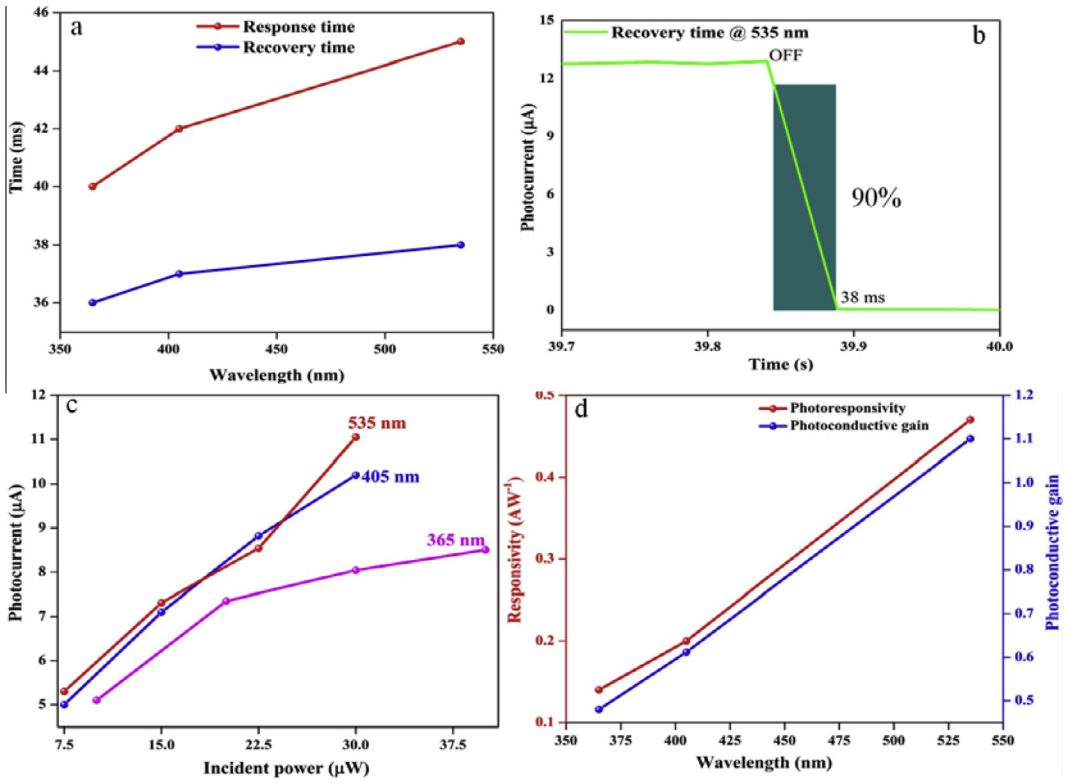

Fig. 7 – Summarized photoresponse result of the p-FLG device. (a) The response and recovery times of the device under UV and visible-light irradiation. (b) The magnification of a single on/off cycle for 535 nm. (c) The power-dependence photoresponse of the p-FLG device. (d) Responsivity and photoconductive gain of the p-FLG device as function of the incident light source. (A colour version of this figure can be viewed online.)

did the low energy photons (405, and 535 nm light). Soon after the light was switched off, the recovery process was initiated, with the device reaching 10% of its maximum value within 38 ms, as shown in Fig. 7b. The fast recovery observed for the high-energy photons was attributed to recombination through interband transitions. In contrast, the existence of a dominant intraband transition created an increment in the recovery time [13]. However, the response and recovery time of our device was comparable to that in previous reports [13,43]. The photocurrent as a function of incident power with various illumination wavelengths is shown in Fig. 7c. The photocurrent of the device increased linearly with the incident power for all illumination wavelengths.

The most significant parameters to determine the capability of a photodetector or photoconductor is responsivity (R), which depends on the electrical output to the optical input. R is defined as,

$$R(AW^{-1}) = \frac{(I_{light} - I_{dark})}{P_{opt}} = \eta\left(\frac{q\lambda}{hc}\right)G \quad (1)$$

where, I_{light}, I_{dark}, P_{opt}, η, q, λ h, c and G are the current under illumination, current in dark, incident light power, quantum efficiency, electronic charge, light wavelength, Planck's constant, speed of light, and photoconductive gain, respectively. The responsivity of p-FLG device is estimated using Eq. (1), assuming that $\eta = 1$ at a bias voltage of 0 V for the three different wavelengths shown in Fig. 7d. The high responsivity of 0.47, 0.20 and 0.14 AW^{-1} was obtained for 535, 405, and 365 nm wavelengths, respectively. This high photoresponsivity of p-FLG was achieved through electron–hole pair generation by direct PE and the impact ionization process. Meanwhile, the photoconductive gain for p-FLG also calculated and the values are 1.1, 0.61, and 0.48 corresponds to the 535, 405, and 365 nm illumination wavelength, respectively (Fig. 7d). The photoconductive gain increased with respect to the wavelength, which arose due to the increment in carrier MEG efficiency. When the photo-excited electron arrived at the higher-energy level in the conduction band, it began to scatter into the lower energy levels of the conduction band by impact ionization. This generated more excitons, which led to the capture of the electron in the MGB state, resulting in a higher photoconductive gain [13]. In case of high-energy (UV) photons the responsivity and the photoconductive gain values are small when compare to the lower-energy (visible light) photons, this due to photoinduced molecular desorption [29], from defected graphene surface. The plasma-induced structural defects open up a new way to tailor graphene properties to specific optoelectronic applications.

4. Conclusions

We have demonstrated a simple, novel way to harvest the optoelectronic properties of graphene layers based on atmospheric plasma irradiation. Plasma-induced structural defects and electrical changes were systematically studied. The

photoconducting ability of p-FLG was tested under both visible and ultraviolet light illumination. A maximum photoresponsivity of 0.47 AW^{-1} and photoconductive gain of 1.1 were achieved with 535 nm light illumination, for a bias voltage of 0 V. This defect-induced photoresponse of graphene layers opens up exciting applications in graphene-based optoelectronics devices.

Acknowledgements

This research was supported by Basic Science Research Program through the National Research Foundation of Korea (NRF) funded by the Ministry of Science, ICT & Future Planning (2013R1A1A2064471).

Appendix A. Supplementary data

Supplementary data associated with this article can be found, in the online version, at http://dx.doi.org/10.1016/j.carbon.2014.02.027.

REFERENCES

[1] Geim AK, Novoselov KS. The rise of graphene. Nat Mater 2007;6:183–91.
[2] Novoselov KS, Geim AK, Morozov SV, Jiang D, Zhang Y, Dubonos SV, et al. Electric field effect in atomically thin carbon films. Science 2004;306:666–9.
[3] Zhang EX, Newaz AKM, Wang B, Zhang CX, Fleetwood DM, Bolotin KI, et al. Ozone-exposure and annealing effects on graphene-SiO_2 transistors. Appl Phys Lett 2012;101:121601.
[4] Sargent EH. Photodetectors: a sensitive pair. Nat Nanotechnol 2012;7:349–50.
[5] Lemme MC, Koppens FHL, Abram LF, Rudner MS, Park H, Levitov LS, et al. Gate-activated photoresponse in a graphene p–n junction. Nano Lett 2011;11:4134–7.
[6] Gaborl NM, Song JCW, Ma Q, Nair NL, Taychatanapat T, Watanabe K, et al. Hot carrier–assisted intrinsic photoresponse in graphene. Science 2011;334:648–52.
[7] Song JCW, Rudner MS, Marcus CM, Levitov LS. Hot carrier transport and photocurrent response in graphene. Nano Lett 2011;11:4688–92.
[8] Echtermeyer TJ, Britnell L, Jasnos PK, Lombardo A, Gorbachev RV, Grigorenko AN, et al. Strong plasmonic enhancement of photovoltage in graphene. Nat Commun 2011;2:458.
[9] Koppens FHL, Chang DE, Garcia de Abajo FJ. Graphene plasmonics: a platform for strong light–matter interactions. Nano Lett 2011;11:3370–7.
[10] Thongrattanasiri S, Koppens FHL, Garcia de Abajo FJ. Complete optical absorption in periodically patterned graphene. Phys Rev Lett 2012;108:047401.
[11] Furchi M, Urich A, Pospischil A, Lilley G, Unterrainer K, Detz H, et al. Microcavity-integrated graphene photodetector. Nano Lett 2012;12:2773–7.
[12] Engel M, Steiner M, Lombardo A, Ferrari AC, Löhneysen HV, Avouris P, et al. Light–matter interaction in a microcavity-controlled graphene transistor. Nat Commun 2012;3:906.
[13] Zhang Y, Liu T, Meng B, Li X, Liang G, Hu X, et al. Broadband high photoresponse from pure mono graphene photodetector. Nat Commun 2013;4:1811.
[14] Konstantatos G, Howard I, Fischer A, Hoogland S, Clifford J, Klem E, et al. Ultrasensitive solution-cast quantum dot photodetectors. Nature 2006;442:180–3.
[15] Konstantatos G, Badioli M, Gaudreau L, Osmond J, Bernechea M, Pelayo Garcia de Arquer F, Gatti F, Koppens FHL. Hybrid graphene–quantum dot phototransistors with ultrahigh gain. Nat Nanotechnol 2012;7:363–8.
[16] Bonaccorso F, Sun Z, Hasan T, Ferrari AC. Graphene photonics and optoelectronics. Nat Photon 2010;4:611–22.
[17] Kitagawa K, Yamakawa K, Fukushima H, Yoshiie T, Hayashi Y, Yoshida H, et al. Ion-irradiation experiment for the fundamental studies of damage evolution of fusion materials. J Nucl Mater 1985;133–134:395–9.
[18] Al-Harthi SH, Kara'a A, Hysen T, Elzain M, Al-Hinai AT, Myint MTZ. Evolution of surface morphology and electronic structure of few layer graphene after low energy Ar^+ ion irradiation. Appl Phys Lett 2012;101:213107.
[19] Zhou YB, Liao ZM, Wang YF, Duesberg GS, Xu J, Fu Q, et al. Ion irradiation induced structural and electrical transition in graphene. J Chem Phys 2010;133:2347031–5.
[20] Cheng YC, Kaloni TP, Zhu ZY, Schwingenschlögl U. Oxidation of graphene in ozone under ultraviolet light. Appl Phys Lett 2012;101:073110.
[21] Fang Z, Wang Y, Liu Z, Schlather A, Ajayan PM, Koppens FHL, et al. Plasmon-induced doping of graphene. ACS Nano 2012;6:10222–8.
[22] Nourbakhsh A, Cantoro M, Klekachev AV, Pourtois G, Vosch T, Hofkens J, et al. Single layer vs bilayer graphene: a comparative study of the effects of oxygen plasma treatment on their electronic and optical properties. J Phys Chem C 2011;115:16619–24.
[23] Singh AK, Penev ES, Yakobson BI. Vacancy clusters in graphene as quantum dots. ACS Nano 2010;4:3510–4.
[24] Woo SO, Teizer W. The effect of electron induced hydrogenation of graphene on its electrical transport properties. Appl Phys Lett 2013;103:041603.
[25] Tao H, Moser J, Alzina F, Wang Q, Sotomayor-Torres CM. The morphology of graphene sheets treated in an ozone generator. J Phys Chem C 2011;115:18257–60.
[26] Childres I, Jauregui LA, Tian J, Chen YP. Effect of oxygen plasma etching on graphene studied using Raman spectroscopy and electronic transport measurements. New J Phys 2011;13:025008.
[27] Teweldebrhan D, Balandin AA. Modification of graphene properties due to electron-beam irradiation. Appl Phys Lett 2009;94:013101.
[28] Eren B, Hug D, Marot L, Pawlak R, Kisiel M, Steiner R, et al. Pure hydrogen low-temperature plasma exposure of HOPG and graphene: graphene formation. Beilstein J. Nanotechnol. 2012;3:852–9.
[29] Lee SW, Mattevi C, Chhowalla M, Mohan Sankaran R. Plasma-assisted reduction of graphene oxide at low temperature and atmospheric pressure for flexible conductor applications. J Phys Chem Lett 2012;3:772–7.
[30] Sun P, Zhu M, Wang K, Zhong M, Wei J, Wu D, et al. Photoinduced molecular desorption from graphene films. Appl Phys Lett 2012;101:053107.
[31] Peltekis N, Kumar S, McEvoy N, Lee K, Weidlich A, Duesberg GS. The effect of downstream plasma treatments on graphene surfaces. Carbon 2012;50:395–403.
[32] Choi K, Lim J, Rani JR, Yoon HS, Oh J, Hong T, et al. Terahertz and optical study of monolayer graphene processed by plasma oxidation. Appl Phys Lett 2013;102:131901.
[33] Yeo S, Choi C, Jang CW, Lee S, Jhon YM. Sensitivity enhancement of carbon nanotube based ammonium ion sensors through surface modification by using oxygen plasma treatment. Appl Phys Lett 2013;102:073108.

[34] Su Y, Pei S, Du J, Liu WB, Liu C, Cheng HM. Patterning flexible single-walled carbon nanotube thin films by an ozone gas exposure method. Carbon 2013;53:4–10.
[35] Yan JA, Chou MY. Oxidation functional groups on graphene: structural and electronic properties. Phys Rev B 2010;82:125403.
[36] Han N, Cuong TV, Han M, Ryu BD, Chandramohan S, Park JB, et al. Improved heat dissipation in gallium nitride light-emitting diodes with embedded graphene oxide pattern. Nat Commun 2013;4:1452.
[37] Breusing M, Ropers C, Elsaesser T. Ultrafast carrier dynamics in graphite. Phys Rev Lett 2009;102:086809.
[38] Tielrooij KJ, Song JCW, Jensen SA, Centeno A, Pesquera A, Elorza AZ, et al. Photoexcitation cascade and multiple hot-carrier generation in graphene. Nat Phys 2013;9:248–52.
[39] Winzer T, Knorr A, Malic E. Carrier multiplication in graphene. Nano Lett 2010;10:4839–43.
[40] Sukhovatkin V, Hinds S, Brzozowski L, Sargent EH. Colloidal quantum-dot photodetectors exploiting multiexciton generation. Science 2009;324:1542–4.
[41] Schaller RD, Klimov VI. High efficiency carrier multiplication in PbSe nanocrystals implications for solar energy conversion. Phys Rev Lett 2004;92:186601.
[42] Ellingson RJ, Beard MC, Johnson JC, Yu P, Micic OI, Nozik AJ, et al. Highly efficient multiple exciton generation in colloidal PbSe and PbS quantum dots. Nano Lett 2005;5:865–71.
[43] Sun Z, Liu Z, Li J, Tai G, Lau SP, Yan F. Infrared photodetectors based on CVD-grown graphene and PbS quantum dots with ultrahigh responsivity. Adv Mater 2012;24:5878–83.